Numerical Simulation of Natural Convection in a Cavity Filled with a Non-Newtonian Ternary Hybrid Nanofluid

Messaouda ALLAM[1*], Mohammed ELMIR[1,2], Razli MEHDAOUI[1,2], Abdelkarim MISSOUM[1]
[1]Energetics in Arid zones Laboratory (ENERGARID), faculty of Technology, TAHRI Mohamed University of Bechar, P. O. Box 417, Algeria
[2]Mechanics, Modeling and Experimentation Laboratory (L2ME), Faculty of Technology, TAHRI Mohamed University of Bechar, P. O. Box 417, Algeria

Abstract

The present work proposes a comprehensive numerical study of natural convection within a non-Newtonian ternary hybrid nanofluid ($Cu + Al_2O_3 + MWCNT + water$) confined in a two-dimensional square enclosure. The vertical side walls are assumed to be adiabatic, while the horizontal walls are maintained at distinct constant temperatures - one hot and one cold - thereby establishing a thermal gradient that drives the flow. The complete set of governing equations, namely mass conservation, momentum, and energy, incorporating the non-Newtonian apparent viscosity, is solved numerically using the finite element method with an implicit Galerkin scheme. The rheological behavior of the fluid is described by the Power-Law model. A systematic parametric analysis is conducted to evaluate the combined effects of the Rayleigh number (Ra), nanoparticle volume fractions (φ_i), and the power-law behavioral index (n) on the thermal and dynamic fields, as well as on heat transfer intensity. The numerical results reveal that incorporating nanoparticles into the base fluid significantly enhances the thermal efficiency of the system. Furthermore, the non-Newtonian character of the fluid exerts a decisive influence on the flow structure and on the intensity of convective heat exchange.

Keywords: Ternary hybrid nanofluid; non-Newtonian fluid; Natural convection; Heat transfer enhancement; Pseudoplastic fluid; Rayleigh number; Nusselt number; Finite Elements.

INTRODUCTION

Recent advances in nanotechnology have opened promising avenues for optimizing heat transfer systems. By enriching a conventional heat-transfer fluid with metallic or non-metallic nanoparticles, it becomes possible to substantially increase its effective thermal conductivity and thereby improve the energy performance of thermal equipment. This concept, originally introduced by (Choi, S.U. et al., 1995). has since attracted growing interest within the scientific community, particularly in applications involving confined geometries.

Natural convection in closed enclosures is a fundamental configuration encountered in numerous industrial and energy-related contexts: cooling of electronic components, solar thermal systems, biomedical applications, chemical reactors, as well as manufacturing processes for polymers and optical fibers. The study of this phenomenon in non-Newtonian configurations is of particular interest because many industrial fluids - such as colloidal suspensions, biological fluids, gels, and slurries - do not obey Newton's law of viscosity. In this context, several categories of rheological models have been proposed in the literature to describe the flow behavior of non-Newtonian fluids, among which one can cite the Carreau, Cross, Williamson, Maxwell, Oldroyd-B, Jeffrey, and power-law models. The latter, owing to its simplicity and its ability to reproduce pseudoplastic and dilatant behaviors, is widely adopted in numerical studies.

(Keshavarz M. et al., 2014). conducted a computational fluid dynamics (CFD) numerical investigation of heat transfer by forced convection of non-Newtonian nanofluids flowing in a horizontal tube with an isothermal wall under turbulent conditions. Three types of nanoparticles (Al_2O_3, TiO_2, and CuO) dispersed in an aqueous carboxymethylcellulose solution were considered, with particle sizes of 10, 25, and 40 nm. The influence of nanoparticle type and Peclet number on the convective heat transfer coefficient was systematically examined. An empirical Nusselt number correlation expressed in terms of relevant dimensionless numbers was established from simulation results, with accuracy within approximately 12% of experimental data from the literature. (S. Mohsenian et al., 2017) studied the flow of a non-Newtonian nanofluid through a converging microchannel. Their investigation focused on the dispersion of TiO_2 nanoparticles in an aqueous carboxymethylcellulose (CMC) solution, which imparts pseudoplastic behavior to the mixture. The finite volume method was used to solve the governing equations. Results indicate that increasing both the nanoparticle volume fraction and the Reynolds number leads to simultaneous improvement in heat transfer and flow velocity. (Fendigil F.S. et al., 2023) published a comprehensive bibliographic review dedicated to the applications of non-Newtonian nanofluids for convection in cavities subjected to an external magnetic field. The authors examine the influence of the magnetic field on the thermal conductivity and viscosity of nanofluids, and highlight current gaps in the literature while identifying research directions for optimizing the design of thermal systems based on these fluids. (Tarakaramu N. et al., 2023) examined the three-dimensional flow of a non-Newtonian nanofluid in the presence of nonlinear thermal radiation and heat absorption, over a stretching surface subjected to a magnetic field and convective boundary conditions. The coupled system of ordinary differential equations was solved numerically using the fourth-order Runge-Kutta-Fehlberg method. Results demonstrate significant modifications to the velocity and temperature profiles as a function of the problem parameters. (Akbar N.S et al., 2023) addressed the numerical analysis of non-Newtonian nanofluids under double-diffusion conditions, over a continuously stretching surface. The partial differential equations governing the problem were transformed into dimensionless form and then solved numerically. The impact of the various parameters on the velocity, temperature, and concentration profiles was highlighted. (Nabwey H.A. et al., 2023) proposed a comprehensive review of non-Newtonian models applied to nanofluids, supported by an in-depth statistical analysis of the literature. Their study reveals, in particular, that 25% of the reviewed works treat nanofluids based on Newtonian base fluids as non-Newtonian fluids, underscoring the importance of consistency in rheological modelling. Asadi A. and al. (2020) conducted an experimental study on the rheological characterization and dynamic viscosity of a CuO-TiO_2/water hybrid nanofluid. Their measurements showed that the synthesized nanofluid exhibits Newtonian behavior, with maximum dynamic viscosity at a concentration of 1 vol.% and a temperature of 25°C. The authors conclude that this nanofluid represents an attractive alternative to the pure base fluid, owing to its high stability and relatively low production cost. (Jeelani M.B et al., 2023) analyzed the combined effects of solar radiation, wall suction, and magnetohydrodynamics on a Maxwell-type hybrid nanofluid (Al_2O_3-Cu/ethylene glycol). The problem was formulated mathematically as a system of partial differential equations, subsequently reduced to a system of ordinary differential equations by similarity transformation, enabling analysis of the velocity and temperature fields. (Chemloul N.S et al., 2016) numerically investigated natural convection in a square cavity with varied horizontal heating. The influence of the Rayleigh number and nanoparticle volume fraction on heat transfer was examined, revealing a significant improvement in the average Nusselt number with increasing values of both parameters for water-based nanofluids. (Algehyne E.A. et al., 2022) employed the pseudoplastic model to study mass and energy transfer through a trihybrid nanofluid flow over a porous stretching surface. The Darcy-Forchheimer relation is incorporated into the momentum equation to account for porosity effects. The Cattaneo-Christov double-diffusion theories are used for the energy and mass expressions. (Rajesh V. et al., 2023) examined the free convection of a ternary hybrid nanosuspension (Al_2O_3-Ag-CuO/water) in an enclosure with a linearly varying side wall temperature. Their finite element approach demonstrated that the addition of a third nanoparticle species significantly enhances energy transport within the cavity, particularly under uniform heating compared with non-uniform heating. (Riaz S. et al., 2024) developed a 2D mathematical model to analyze heat transfer in a ternary hybrid nanofluid (Al_2O_3, MgO, TiO_2) over a stretching surface, incorporating viscous dissipation and using the Rosseland approximation for radiation. The dimensionless equations were derived by local non-similarity transformation. (Ramzan M. et al., 2023) theoretically examined magnetohydrodynamic ternary hybrid nanofluid flows over cone and wedge geometries. Results indicate that chemical reactions and thermal radiation substantially influence the flow, and that increasing nanoparticle volume fraction enhances heat transfer rates for both geometries.

The primary objective of this contribution is to analyze the influence of control parameters -Rayleigh number, nanoparticle volume fractions, and the power-law behavioral index - on the natural convection of a non-Newtonian ternary hybrid nanofluid in a square cavity.

PHYSICAL AND MATHEMATICAL MODEL

Physical configuration

The geometric configuration considered in this study is a two-dimensional square cavity of side H, as schematically illustrated in Figure 1. The lower wall is maintained at a uniform elevated temperature T_h, while the upper wall is held at a constant cold temperature T_c ($T_h > T_c$). The two vertical walls are assumed to be perfectly thermally insulated (zero-flux condition). The working fluid is a non-Newtonian ternary hybrid nanofluid, assumed to be incompressible, in laminar two-dimensional flow under transient conditions.

In order to render the problem mathematically tractable, the following simplifying assumptions have been adopted:

- The fluid is incompressible and the medium is treated as a continuum;
- The flow is laminar and strictly two-dimensional;
- Viscous dissipation is neglected relative to the other energy terms;
- The Boussinesq approximation is invoked to account for buoyancy effects in the vertical momentum equation.

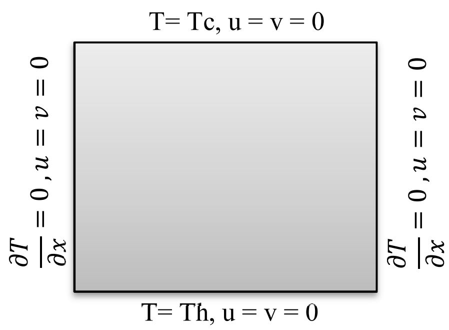

Figure 1. Physical model

Rheological model

Both the base fluid and all nanofluids exhibit shear-thinning (pseudoplastic) rheological behavior. For non-Newtonian fluids of this type, the apparent viscosity is generally described by the power-law model (Hojjat M. et al., 2011). (Kamali R. et al., 2010). according to the expression:

$$\mu_{thnf} = k\dot{\gamma}^{n-1} \tag{1}$$

where k denotes the consistency coefficient, $\gamma^{\cdot}$ the shear rate, and n the behavioral index. For (n<1), the fluid is pseudoplastic; for n = 1, it behaves as a Newtonian fluid; for n > 1, it is dilatant. Rheological parameters are obtained from the literature (Hojjat, M. et al. 2011) as functions of temperature and particle concentration.

Effective properties of the ternary hybrid nanofluid

The effective density, heat capacity, thermal expansion coefficient, viscosity, and thermal conductivity are computed using standard mixture rules extended to three types of nanoparticles.

Density:

$$\rho_{th\,nf} = \varphi_3\rho_3 + (1-\varphi_3)\left[\varphi_2\rho_2 + (1-\varphi_2)[\varphi_1\rho_1 + (1-\varphi_1)\rho_f]\right] \quad (2)$$

Dynamic viscosity (Brinkman, H. C. 1947):

$$\mu_{thnf} = \frac{\mu_f}{(1-\varphi_1)^{2.5}(1-\varphi_2)^{2.5}(1-\varphi_3)^{2.5}} \quad (3)$$

Heat capacity:

$$(\rho C_p)_{th\,nf} = \varphi_3\,(\rho C_p)_3 + (1-\varphi_3)[\varphi_2\,(\rho C_p)_2 + (1-\varphi_2)[\varphi_1(\rho C_p)_1 + (1-\varphi_1)(\rho C_p)_f]] \quad (4)$$

Thermal expansion coefficient:

$$(\rho\beta)_{thnf} = (1-\varphi_3)[(1-\varphi_2)[(1-\varphi_1)(\rho\beta)_f + \varphi_1(\rho\beta)_1] + \varphi_2(\rho\beta)_2] + \varphi_3(\rho\beta)_3 \quad (5)$$

Thermal conductivity (Maxwell–Bruggeman model extended) (Rajesh, V. et al 2023):

$$k_{thnf} = k_{hnf}\,\frac{k_3+2k_{hnf}-2\varphi_2(k_{hnf}-k_3)}{k_3+2k_{hnf}+\varphi_2(k_{hnf}-k_3)} \quad (6)$$

With intermediate expressions for k_{hnf} and k_{nf}.

$$K_{hnf} = k_{nf}\left[\frac{k_2+2k_{nf}-2\varphi_2(k_{nf}-k_2)}{k_2+2k_{nf}+\varphi_2(k_{nf}-k_2)}\right] \quad \text{and} \quad k_{nf} = k_f\left[\frac{k_1+2k_f-2\varphi_1(k_f-k_1)}{k_1+2k_f+\varphi_1(k_f-k_1)}\right]$$

In these expressions, subscripts 1, 2, and 3 refer to the Cu, Al_2O_3, and MWCNT nanoparticles, respectively, while f denotes the base fluid (water).

Dimensional governing equations

Under the Boussinesq approximation (Kamali, R. et al. 2010) and (Moraveji, M.K. et al. 2012), the steady laminar natural convection is described by:

Continuity: $$\frac{\partial u}{\partial x} + \frac{\partial v}{\partial y} = 0 \quad (7)$$

Momentum : $$\rho_{thnf}\left(\frac{\partial u}{\partial t}+u\frac{\partial u}{\partial x}+v\frac{\partial u}{\partial y}\right)=-\frac{\partial p}{\partial x}+\frac{\partial}{\partial x}\left(\mu_{thnf}\nabla u\right) \quad (8)$$

$$\rho_{thnf}\left(\frac{\partial v}{\partial t}+u\frac{\partial v}{\partial x}+v\frac{\partial v}{\partial y}\right)=-\frac{\partial p}{\partial y}+\frac{\partial}{\partial y}\left(\mu_{thnf}\nabla v\right)-\rho_{onf}\,g\left(1-\beta_{thnf}(T_c-T_0)\right) \quad (9)$$

Energy: $$\left(Pc_p\right)_{thnf}\left(\frac{\partial T}{\partial t}+u\frac{\partial T}{\partial x}+v\frac{\partial T}{\partial y}\right)=k_{thnf}\left(\frac{\partial^2 T}{\partial x^2}+\frac{\partial^2 T}{\partial y^2}\right) \quad (10)$$

Dimensionless form

The system of equations (7-10) is written in dimensionless form after introducing the following dimensionless parameters:

$$(X,\ Y)=\frac{(x,\ y)}{H}\ ;\ (U,\ V)=\frac{(u,\ v)H}{\alpha_f}\ ;\ \theta=\frac{T-T_c}{T_H-T_c};\ \tau=\frac{t\alpha_f}{H^2}\ ;\ P=\frac{pH^2}{\rho_{thnf}\alpha_f^2};\ Pr=\frac{v_f}{\alpha_f}.$$

$$Ra=\frac{g\beta_{fb}(T_H-T_c)H^3}{v_f\alpha_f}.$$

The resulting system of these partial differential equations takes the form:

$$\frac{\partial U}{\partial X}+\frac{\partial V}{\partial Y}=0 \quad (11)$$

$$\frac{\rho_{thnf}}{\rho_f}\left(\frac{\partial U}{\partial \tau}+U\frac{\partial U}{\partial X}+V\frac{\partial U}{\partial Y}\right)=-\frac{\partial P}{\partial X}+Pr\frac{\mu_{thnf}}{\mu_f}\left(\frac{\partial^2 U}{\partial X^2}+\frac{\partial^2 U}{\partial Y^2}\right) \quad (12)$$

$$\frac{\rho_{thnf}}{\rho_f}\left(\frac{\partial V}{\partial \tau}+U\frac{\partial V}{\partial X}+V\frac{\partial V}{\partial Y}\right)=-\frac{\partial P}{\partial Y}+Pr\frac{\mu_{thnf}}{\mu_f}\left(\frac{\partial^2 V}{\partial X^2}+\frac{\partial^2 V}{\partial Y^2}\right)+Ra.Pr.\frac{(\rho\beta)_{thnf}}{(\rho\beta)_f}\theta \quad (13)$$

$$\frac{\partial \theta}{\partial \tau}+U\frac{\partial \theta}{\partial X}+V\frac{\partial \theta}{\partial Y}=\frac{k_{thnf}}{k_f}\frac{(\rho C_p)_f}{(\rho C_p)_{thnf}}\left(\frac{\partial^2 \theta}{\partial X^2}+\frac{\partial^2 \theta}{\partial Y^2}\right) \quad (14)$$

Initial conditions: $\tau = 0 : U = V = \theta = 0$

Dimensionless boundaries conditions are summarized in table 1 below.

Table 1. The dimensionless boundary conditions

Walls	Hydrodynamic	Thermal
Lower horizontal wall	U=V=0	$\theta = 1$
Upper horizontal wall	U=V=0	$\theta = 0$
Left vertical wall	U=V=0	$\frac{\partial \theta}{\partial X}=0$
Right vertical wall	U=V=0	$\frac{\partial \theta}{\partial X}=0$

The average Nusselt number, which quantifies the intensity of convective heat transfer relative to pure conduction, is defined as:

$$Nu_a=-\frac{k_{thnf}}{k_{fb}}\int_0^1\left(\frac{\partial \theta}{\partial Y}\right)_{Y=1}dX. \quad (15)$$

NUMERICAL SIMULATION

With the boundary conditions of Table 1 imposed, Eqs. (11)-(14) are solved with a finite element method based on an implicit Galerkin scheme. A mesh-sensitivity study was carried out prior to production runs, since an appropriate discretisation is essential for obtaining accurate, convergent and mesh-independent predictions; several mesh densities were trialled, and a grid of 24500 elements was retained for the reported simulations.

To validate the numerical procedure, the predicted average Nusselt numbers were benchmarked against the classical air-filled square-cavity case ($\varphi_1 = \varphi_2 = \varphi_3 = 0$, Pr = 0.7) for which reference results are available from (De Vahl Davis, 1983). As shown in Table 2, the present results agree closely with this benchmark across the tested Rayleigh numbers, with discrepancies remaining within about 2%.

Table 2. Comparison of the average Nusselt number

Ra	Nu_a (De Vahl Davis, 1983).	Nu_a [Our work]	Difference [%]
10^3	1.117	1.100	1.7
10^4	2.234	2.184	2.2
10^5	4.510	4.600	2.0

RESULTS AND DISCUSSION

The thermophysical properties of water and of the three nanoparticle types used in the simulations (Cu, Al_2O_3 and MWCNT) are listed in Table 3 of the original dataset and were taken from standard reference values.

Table 3. Physical properties of water and nanoparticles

	Water	Cu	Al_2O_3	$MWCNT$
$\rho(kg.m^{-3})$	997.1	8933	3970	1600
Cp$(J.kg^{-1}.K^{-1})$	4179	385	765	796
k$(W.m^{-1}.K^{-1})$	0.613	400	40	3000
$\beta(K^{-1}).10^{-5}$	21	1.67	0.85	0.1

Isotherms

The isotherm patterns obtained for the three Rayleigh numbers considered (10^3, 10^4 and 10^5), together with several behaviour-index values (n) and nanoparticle volume fractions (φi), are presented in Figures 2–4. At Ra = 10^3, the isotherms remain essentially horizontal and parallel irrespective of n and φi, indicating that heat transfer is governed almost entirely by conduction. Once Ra reaches 10^4 with n = 1, the isotherms start to bend near the hot and cold walls, signalling the onset of a stronger vertical temperature gradient; this distortion becomes more pronounced for shear-thinning fluids ($n < 1$) and less pronounced for shear-thickening ones ($n > 1$). Adding nanoparticles also tightens the isotherm spacing close to the walls. At the highest Rayleigh number tested (Ra = 10^5), the isotherms tilt sharply, particularly near the hot wall, where clearly visible thermal plumes develop.

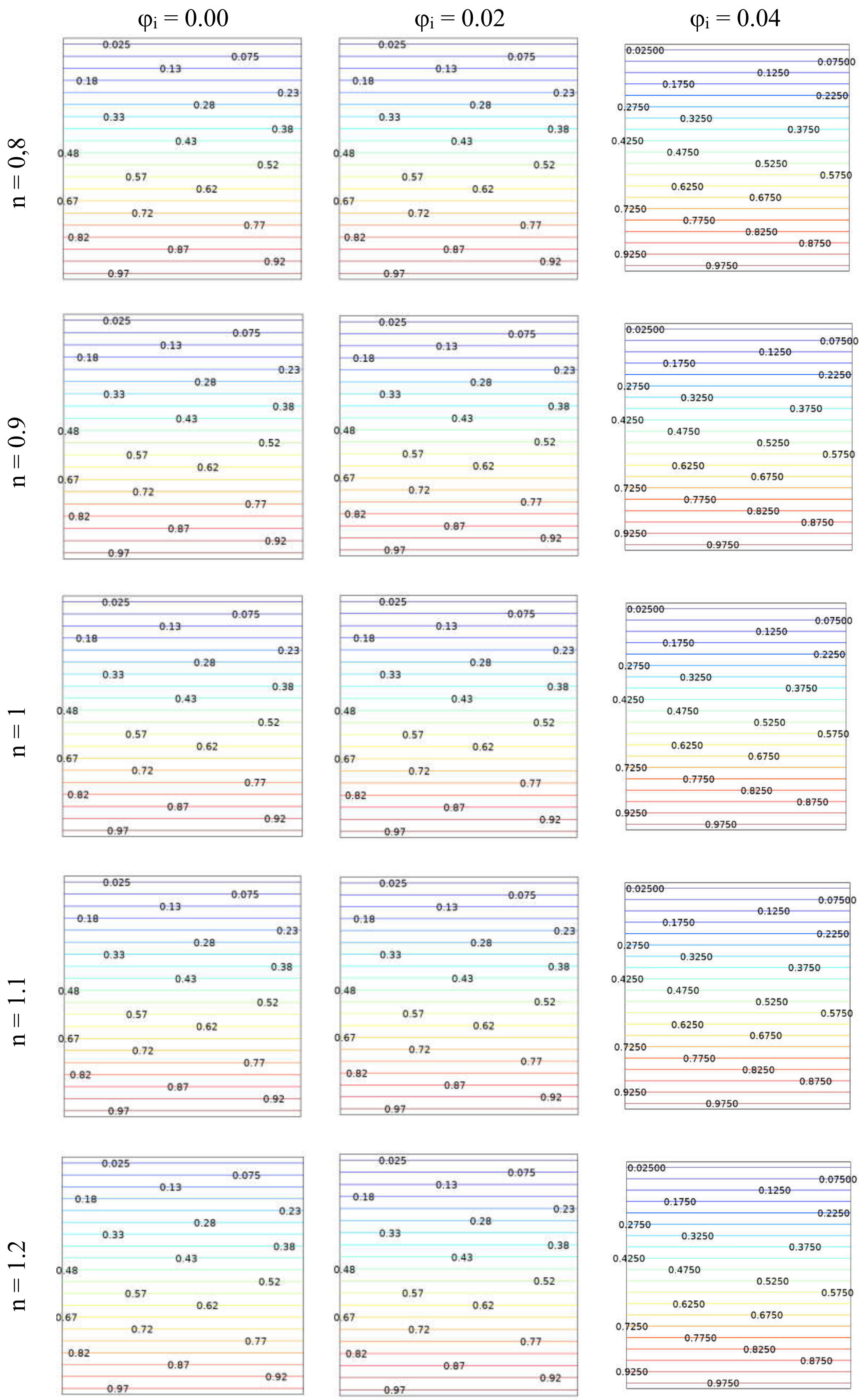

Figure 2. Isotherms for $Ra = 10^3$

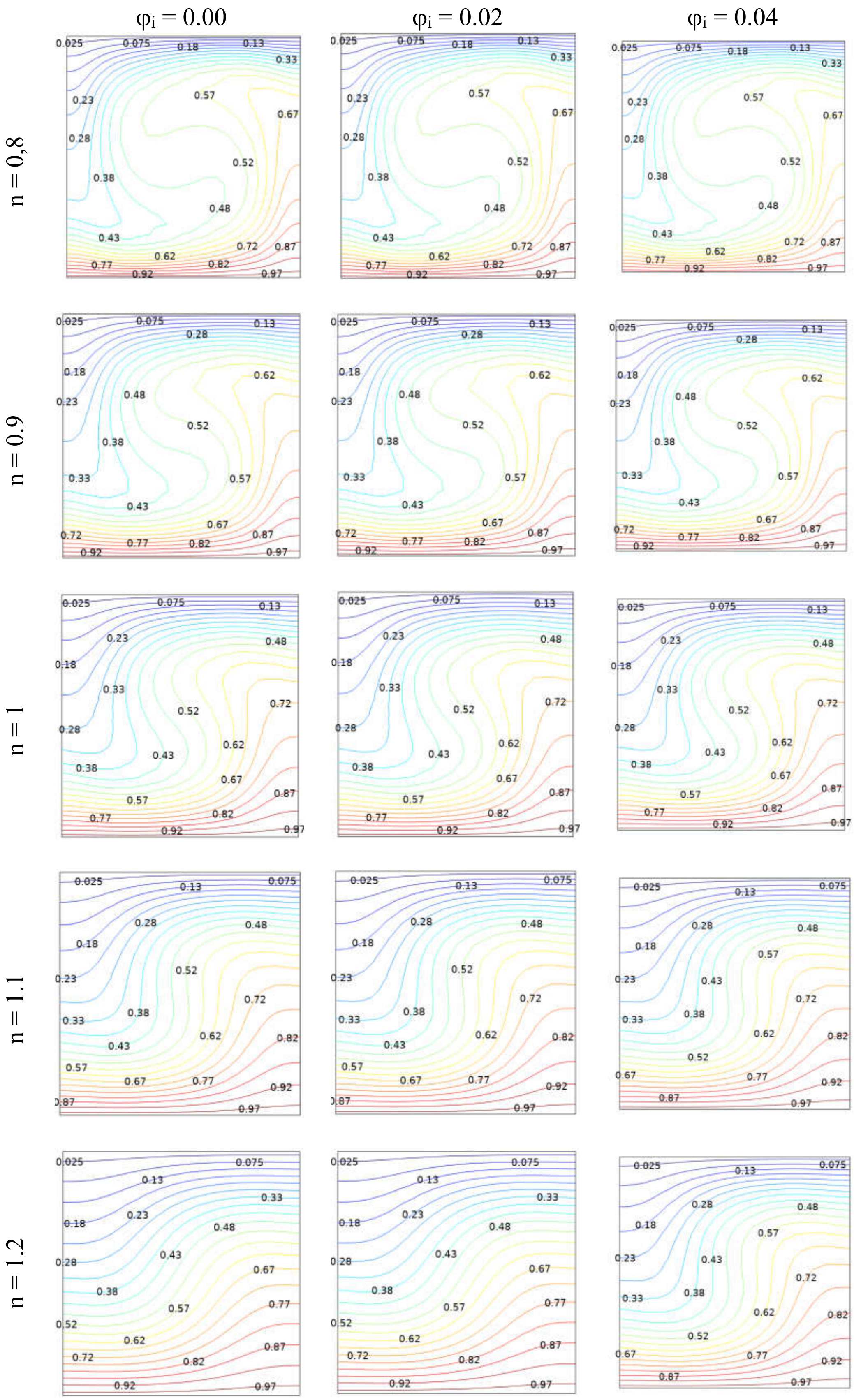

Figure 3. Isotherms for $Ra = 10^4$

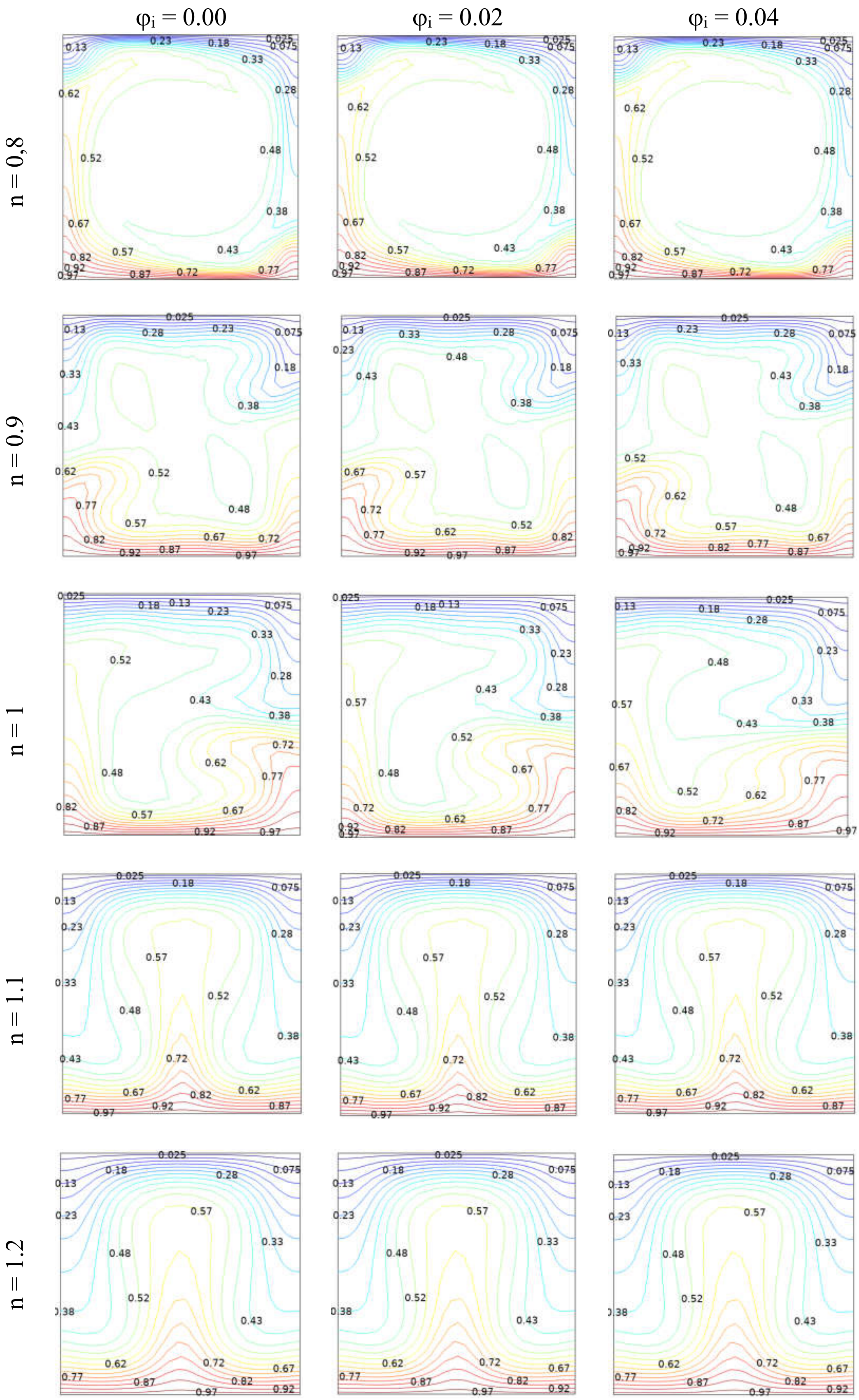

Figure 4. Isotherms for $Ra = 10^5$

Streamlines

Figures 5 and 6 display the streamline fields for the same combinations of Ra, n and φi. At Ra = 10^3, the stream-function values remain close to zero for every combination of n and φi tested, confirming that conduction dominates the heat-transfer process. For Ra = 10^4 with n = 1, the streamlines intensify and the central recirculating cell expands. At Ra = 10^5, the flow can develop a multicellular structure for certain combinations of n and φi, suggesting the onset of flow instabilities.

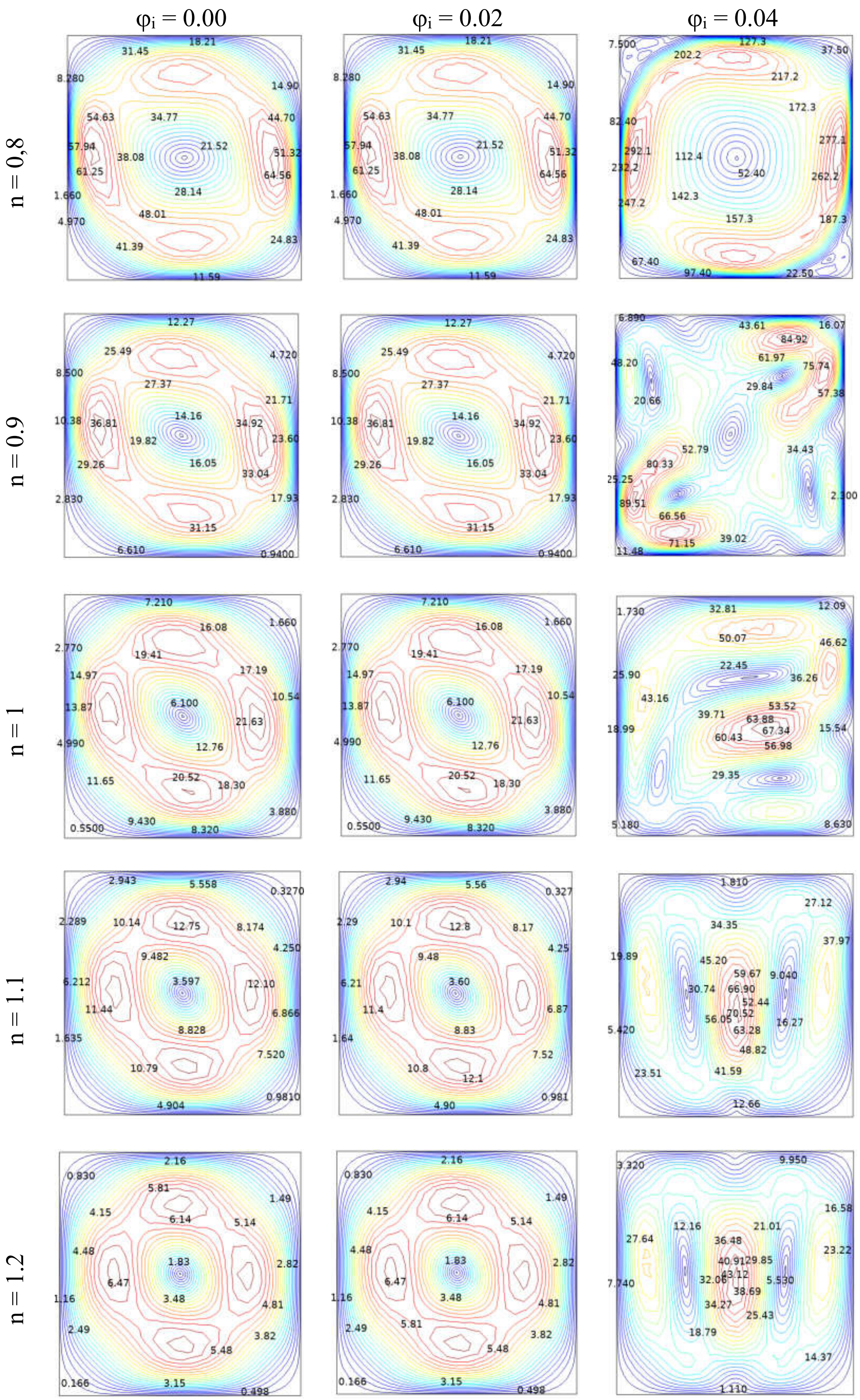

Figure 5. Stream ligne for $Ra = 10^4$

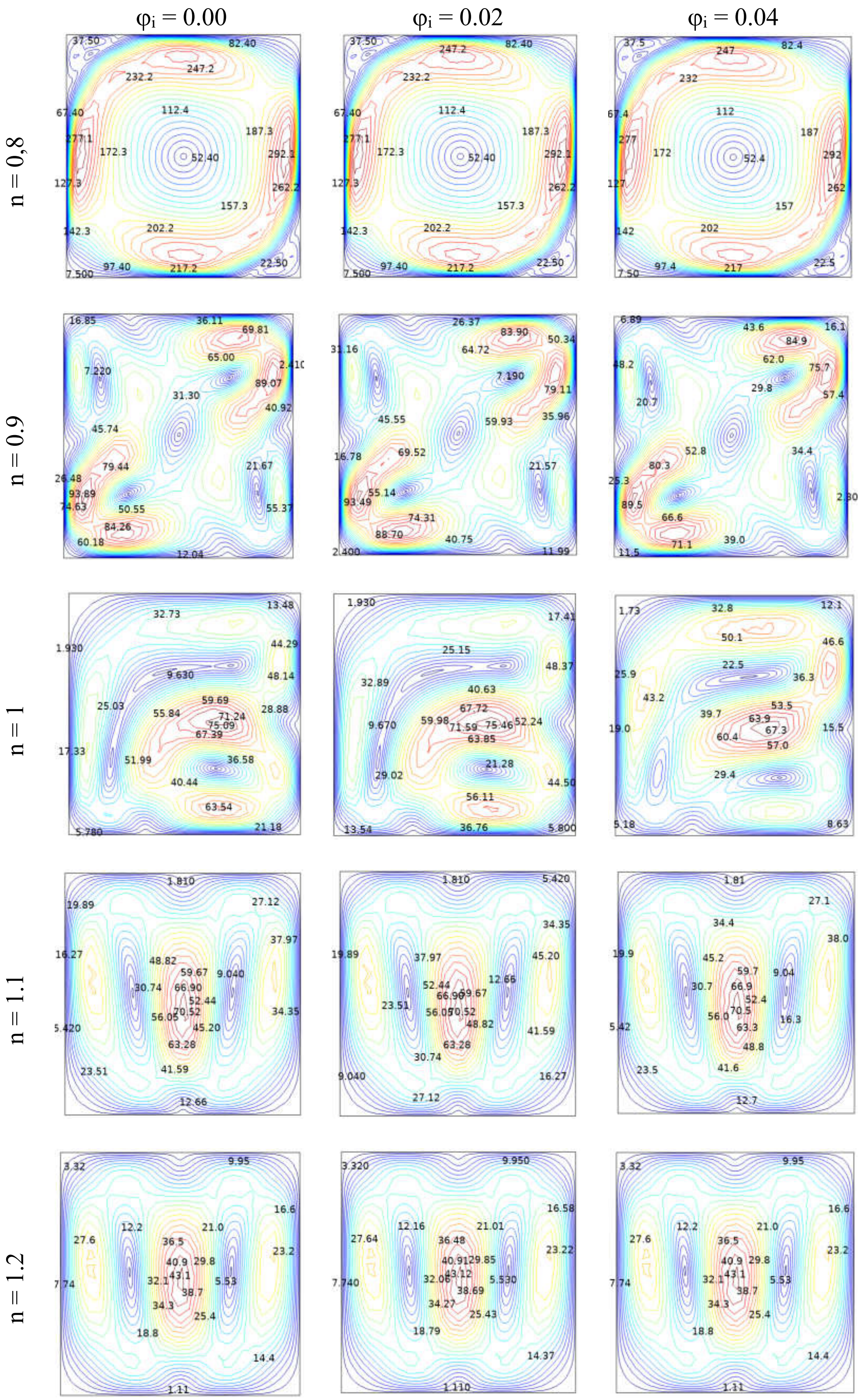

Figure 6. Stream ligne for $Ra = 10^5$

Maximum curent fonction

Ra = 10^3 Ra = 10^4 Ra = 10^5

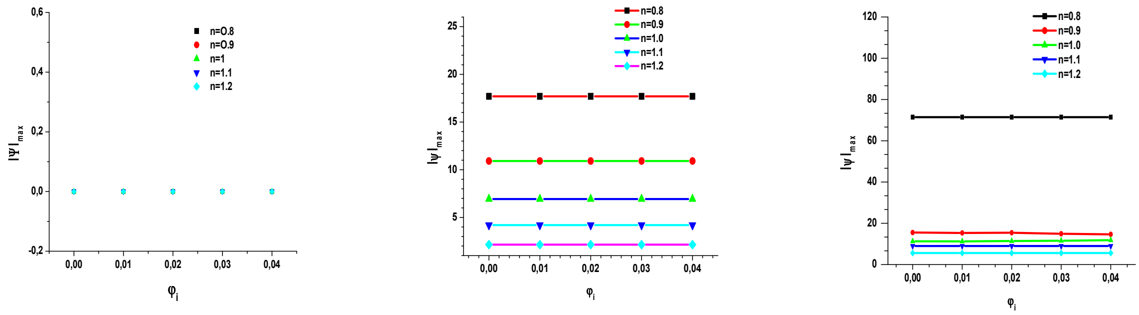

Figure 7. Stream function vs. volume fraction

Figure 7 shows how the absolute maximum value of the stream function varies with nanoparticle volume fraction for the different behaviour indices and Rayleigh numbers examined. The peak stream-function magnitude grows roughly linearly with both the Rayleigh number and the nanoparticle concentration, reflecting a strengthening of the convective motion as either parameter increases.

Average Nusselt number

Ra = 10^3 Ra = 10^4 Ra = 10^5

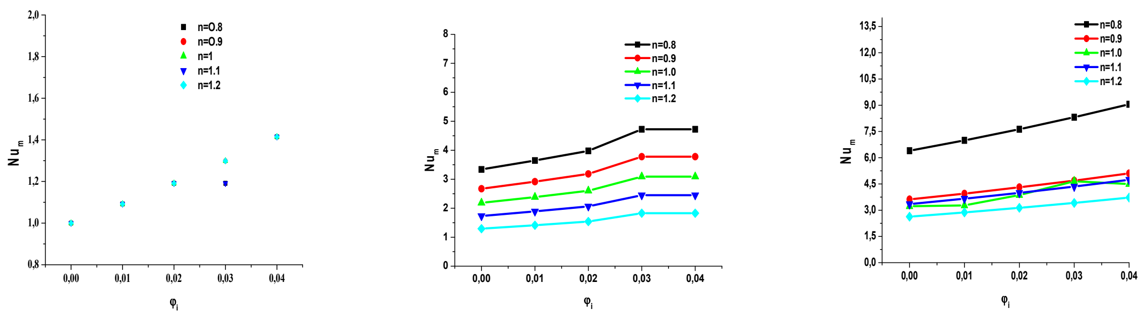

Figure 8.a. Average Nusselt number

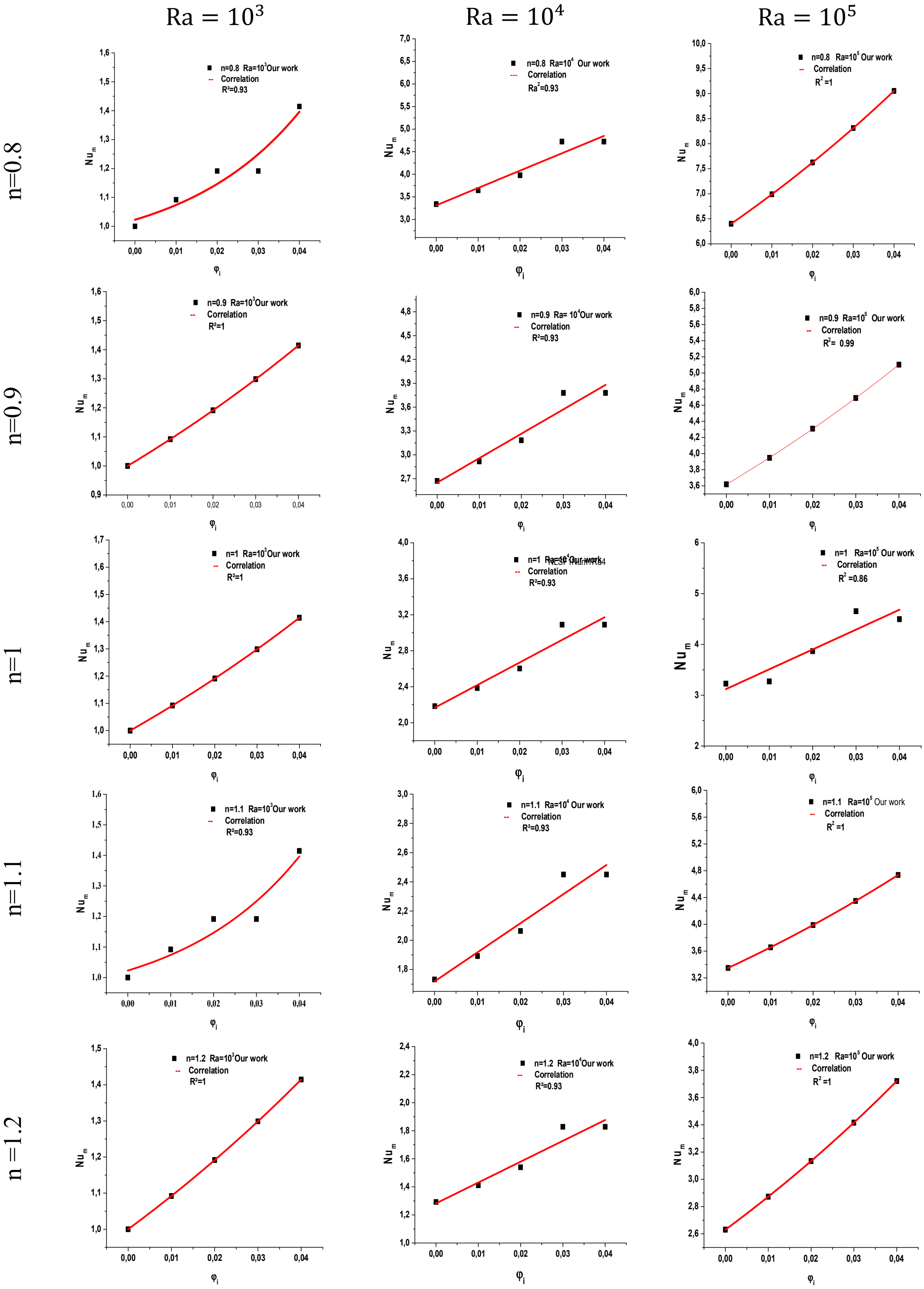

Figure 8.b. Average Nusselt number and correlation

Figure 8(a - b) presents the average Nusselt number as a function of nanoparticle volume fraction for the different Rayleigh numbers and behaviour indices, showing an essentially exponential growth trend. A fitting relation between Nu_a and φi is proposed (Eq. 16), whose coefficients (A, D and Y_0) are themselves expressed as functions of the behaviour index n and the Rayleigh number, as detailed in Eqs. (17)-(19) of the full derivation; these correlations reproduce the simulated Nusselt-number trends with coefficients of determination generally above 0.9. Overall, the average Nusselt number rises with increasing φi and decreases slightly as n increases, consistent with the higher effective viscosity -and hence weaker convection - associated with shear-thickening behaviour.

$$Nu_a = Y_0 + Ae^{\frac{\varphi i}{D}} \tag{16}$$

According to the correlation, the constants A, t, and y0 vary with the different Rayleigh numbers (Ra) as follows:

- Ra=10^3 $\begin{cases} Y_0 = B_{y0} + C_{y0}n \\ A = B_A + C_A\, n \\ D = B_D + C_D\, n \end{cases}$

So:

$$Nu_a = [B_{y0} + C_{y0}n\,] + [B_A + C_A\, n\,\,]e^{\frac{\varphi i}{[B_D + C_D\, n\,]}} \tag{17}$$

$$\begin{cases} Y_0 = 1.324 - 1.057n \\ A = (-0.292) + (1.034)\, n \\ D = (-0.01) + (0.1)\, n \end{cases}$$

$$Nu_a = [1.324 - 1.057n] + [(-0.292) + (1.034)\, n]e^{\frac{\varphi i}{[(-0.01)+(0.1)\, n]}}$$

- Ra=10^4 $\begin{cases} Y_0 = B_{y0} + C_{y0}n \\ A = y_{A0} + A_A e^{\frac{n}{D_A}} \\ D = B_D + C_D\, n \end{cases}$

So:

$$Nu_a = [B_{y0} + C_{y0}n] + [y_{A0} + A_A e^{\frac{n}{t_A}}\,]e^{\frac{\varphi i}{[B_D + C_D\, n]}} \tag{18}$$

$$\begin{cases} Y_0 = 1.324 - 1.057n \\ A = -104.87 + 13498.64e^{\frac{n}{0.4688}} \\ D = (60.79) + (-0.0018)\, n \end{cases}$$

$$Nu_a = [1.324 - 1.057n\,] + [-104.87 + \, 13498.64e^{\frac{n}{(0.4688)}}]e^{\frac{\varphi i}{[(60.79)+(-0.0018)\, n]}}$$

- Ra=10^5 :

- $\begin{cases} Y_0 = y_0 + \frac{A_0}{w^2\sqrt{\frac{\pi}{2}}} e^{-2(n-xc)/w^2} \\ A = y_{A0} + \frac{A_{A0}}{w^2\sqrt{\frac{\pi}{2}}} e^{-2(n-xc)/w^2} \\ D = y_{t0} + \frac{A_{t0}}{w^2\sqrt{\frac{\pi}{2}}} e^{-2(n-xc)/w^2} \end{cases}$ $\begin{cases} y0 = (-0.616) + \frac{(-285.23)}{(0.04)^2\sqrt{\frac{\pi}{2}}} e^{-2(n-1)/(0.04)^2} \\ A = (4.56) + \frac{294.92}{(0.04)^2\sqrt{\frac{\pi}{2}}} e^{-2(n-1)/(0.04)^2} \\ D = 0.13 + \frac{7.47}{(0.04)^2\sqrt{\frac{\pi}{2}}} e^{-2(n-1)/(0.04)^2} \end{cases}$

$$Nu_a = \left[[y_0 + \frac{A_0}{w^2\sqrt{\frac{\pi}{2}}} e^{-2(n-xc)/w^2} \right] + \left[(y_{A0} + \frac{A_{A0}}{w^2\sqrt{\frac{\pi}{2}}}) e^{\left(-2(n-xc)/w^2\right)} \right] e^{\left(\frac{\varphi i}{y_{D0} + \frac{A_{t0}}{w^2\sqrt{\frac{\pi}{2}}} e^{-2(n-xc)/w^2}}\right)} \tag{19}$$

$$Nu_a = \left[(-0.616) + \frac{(-285.23)}{(0.04)^2\sqrt{\frac{\pi}{2}}} e^{-2(n-1)/(0.04)^2} \right] + \left[\left((4.56)\right) + \frac{294.92}{(0.04)^2\sqrt{\frac{\pi}{2}}} e^{-2(n-1)/(0.04)^2} \right] \left[e^{\left(\frac{\varphi i}{(0.13) + \frac{(7.47)}{(0.04)^2\sqrt{\frac{\pi}{2}}} e^{-2(n-1)/(0.04)^2}}\right)} \right]$$

CONCLUSION

A numerical investigation of natural convection of a non-Newtonian ternary hybrid nanofluid (Cu + Al_2O_3 + MWCNT + water) in a square cavity has been carried out using the finite element method. The main findings can be summarised as follows: the ternary hybrid suspension provides a marked enhancement of heat transport thanks to the combined contribution of its three nanoparticle constituents; the power-law behaviour index, representing the non-Newtonian character of the fluid, has a significant effect on both momentum and energy transfer, with shear-thinning fluids (lower n) favouring stronger convection; and increasing either the Rayleigh number or the nanoparticle volume fraction intensifies the circulation and raises the heat-transfer rate. These results suggest that careful tuning of nanoparticle composition and of the rheological properties of the carrier fluid offers a practical route to optimising thermal systems for applications such as electronic-component cooling and photovoltaic-panel thermal management.

References

Akbar, N. S., & Mallawi, F. O. (2023). Numerical analysis of non-Newtonian nanofluids under double-diffusive regimes. Frontier in Materials, 10, Article 1248849. https://doi.org/10.3389/fmats.2023.1248849

Algehyne, E. A., Alrihieli, H. F., Bilal, M., Saeed, A., & Weera, W. (2022). Numerical approach toward ternary hybrid nanofluid flow using variable diffusion and Non-Fourier's concept. ACS Omega, 7(33), 29380–29390. https://doi.org/10.1021/acsomega.2c03634

Asadi, A., Alarifi, I. M., & Foong, L. K. (2020). An experimental study on characterization, stability and dynamic viscosity of CuO–TiO_2/water hybrid nanofluid. Journal of Molecular Liquids, 307, 112987. https://doi.org/10.1016/j.molliq.2020.112987

Brinkman, H. C. (1947). *The viscosity of concentrated suspensions and solutions*. Journal of Chemical Physics, 20, 571–581.

Chemloul, N. S., & Belmiloud, M. A. (2016). Effet des nanoparticules sur l'amélioration du transfert thermique dans une cavité carrée. Revue des Énergies Renouvelables, 19(3), 397–408.

Choi, S.U.; Eastman, J.A. (1995). Enhancing Thermal Conductivity of Fluids with Nanoparticles. Argonne National Lab (ANL) : Argonne, IL, USA, Volume 231, pp. 99–106.

De Vahl Davis, G. (1983). Natural convection of air in a square cavity: A benchmark numerical solution. International Journal for Numerical Methods in Fluids, 3(3), 249–264. https://doi.org/10.1002/fld.1650030305

Fendigil, F. S., Öztop, H. F., Abu-Hamdeh, N., Selimefendigil, F., & Ali, M. E. (2023). A review on non-Newtonian nanofluid applications for convection in cavities under magnetic field. Symmetry, 15(1), 41. https://doi.org/10.3390/sym15010041

Haneef, M., Nawaz, M., Alharbi, S. O., & Elmasry, Y. (2021). Cattaneo–Christov heat flux theory and thermal enhancement in hybrid nano Oldroyd-B rheological fluid in the presence of mass transfer. International Communications in Heat and Mass Transfer, 126, 105344. https://doi.org/10.1016/j.icheatmasstransfer.2021.105344

Hojjat, M., Etemad, S. G., Bagheri, R., & Thibault, J. (2011). Turbulent forced convection heat transfer of non-Newtonian nanofluids. Experimental Thermal and Fluid Science, 35(7), 1351–1356. https://doi.org/10.1016/j.expthermflusci.2011.04.015

Hojjat, M., Etemad, S. G., Bagheri, R., & Thibault, J. (2011). Rheological characteristics of non-Newtonian nanofluids: Experimental investigation. International Communications in Heat and Mass Transfer, 38(2), 144–148. https://doi.org/10.1016/j.icheatmasstransfer.2010.11.004

Huminic, G., & Huminic, A. (2018). Hybrid nanofluids for heat transfer applications: A state-of-the-art review. International Journal of Heat and Mass Transfer, 125, 82–103. https://doi.org/10.1016/j.ijheatmasstransfer.2018.04.059

Jeelani, M. B., & Abbas, A. (2023). Al_2O_3–Cu/ethylene glycol-based magnetohydrodynamic non-Newtonian Maxwell hybrid nanofluid flow with suction effects in a porous space: Energy saving by solar radiation. Symmetry, 15(9), 1794. https://doi.org/10.3390/sym15091794

Kamali, R., & Binesh, A. R. (2010). Numerical investigation of heat transfer enhancement using carbon nanotube-based non-Newtonian nanofluids. International Communications in Heat and Mass Transfer, 37(9), 1153–1157. https://doi.org/10.1016/j.icheatmasstransfer.2010.06.002

Keshavarz Moraveji, M., & Beheshti, A. R. (2014). CFD study of the turbulent forced convective heat transfer of non-Newtonian nanofluid. Iranian Journal of Chemical Engineering, 11(2), 1–13.

Moraveji, M. K., & Hejazian, M. (2012). Modeling of turbulent forced convective heat transfer and friction factor in a tube for Fe_3O_4 magnetic nanofluid with computational fluid dynamics. International Communications in Heat and Mass Transfer, 39(9), 1293–1298. https://doi.org/10.1016/j.icheatmasstransfer.2012.07.012

Nabwey, H. A. (2023). A comprehensive review of non-Newtonian nanofluid heat transfer. Symmetry, 15(2), 362. https://doi.org/10.3390/sym15020362

Rajesh, V., & Sheremet, M. A. (2023). Natural convection of ternary hybrid nanofluid in a differential-heated enclosure with a non-uniformly heated wall. Micromachines, 14(5), 1049. https://doi.org/10.3390/mi14051049

Rajesh, V., & Sheremet, M. A. (2023).. Free Convection in a Square Ternary Hybrid Nanoliquid Chamber with Linearly Heating Adjacent Walls. Nanomaterials, **13**(21), 2860. https://doi.org/10.3390/nano13212860

Ramzan, M., Kumam, P., Waini, I., Abu Bakar, S., & Alghamdi, M. (2023). A theoretical analysis of the ternary hybrid nanofluid flows over a non-isothermal and non-isosolutal multiple geometries. Heliyon, 9(4), e14875. https://doi.org/10.1016/j.heliyon.2023.e14875

Riaz, S., Afzaal, M. F., Wang, Z., Jan, A., & Farooq, U. (2024). "Numerical heat transfer of non-similar ternary hybrid nanofluid flow over linearly stretching surface". Numerical Heat Transfer, Part A: Applications. Volume 85, Issue 23 (2024), pages 4021–4035

Tarakaramu, N., & Satya Narayana, P. V. (2023). Convective conditions on 3D magnetohydrodynamic (MHD) non-Newtonian nanofluid flow with nonlinear thermal radiation and heat absorption: A numerical analysis. Journal of Nanofluids, 12(2), 448–457. https://doi.org/10.1166/jon.2023.1990

S. Mohsenian, A. Ramiarand, A. Ranjbar. (2017). Numerical investigation of non-Newtonian nanofluid flow in a converging microchannel. Journal of Mechanical Science and Technology 31(1) 385~391. DOI 10.1007/s12206-016-1240-0

NOMENCLATURE

C_p Specific heat at constant pressure, J$kg^{-1}K^{-1}$
H Length of square enclosure, m
G Gravitational acceleration, ms^{-2}
N Power Law index
Nu Average Nusselt number
Pr Prandtl number
Ra Rayleigh number
T Fluid temperature, K
Tc Cooled wall temperature, K
Th Hot wall temperature, K
u Velocity component in x-direction, ms^{-1}
U Dimensionless velocity component in x-direction
v Velocity component in y-direction, ms^{-1}
V Dimensionless velocity component in y-direction
x Spatial coordinate along horizontal wall, m
X Dimensionless spatial coordinate along horizontal
y Spatial coordinate along vertical
Y Dimensionless spatial coordinate along vertical
ρ Density, kg m^{-3}

Greek symbols

β	Volumetric thermal expansion coefficient (k^{-1})
μ	Dynamic viscosity, Pa s
v	Kinematic viscosity , m^2s^{-1}
φ_1	Cu nanoparticles volume fraction
φ_2	Al_2O_3 nanoparticles volume fraction
φ_3	MWCNT nanoparticles volume fraction
θ	Dimensionless temperature

Subscripts

f	Base fluid
nf	Nanofluid
hnf	Hybrid Nanofluid

thnf	Ternary hybrid Nanofluid